Adaptive Wavelet Collocation for Elasticity: First Results

Silvia Bertoluzza* and Luis Castro†

Abstract

After recalling the definition and main ideas of the adaptive collocation scheme introduced in [26, 4], we apply it to some test problems arising in two dimensional elasticity, and compare the results obtained with classical finite element methods.

1 Introduction

The solution of many differential problems is very smooth in a large part of the domain, while being globally not as smooth. In order to approximate it in an optimal way the need arises of using high order methods, capable of taking advantage of the local smoothness of the solution by using a coarse grid in the greatest part of the domain, but capable, on the other hand of coping with singularities.

Among the methods that display this potential one can count the methods based on wavelet bases and multiscale analysis. Such bases allow on one hand to design methods of arbitrarily high order, and on the other hand they display a local behavior, allowing one to take into account the presence of singularities by locally refining the approximation space.

Even more, such bases actually provide a singularity detection tool that has been successfully employed in designing adaptive schemes for the numerical solution of several classes of differential equations [20, 4, 26, 25, 8, 23].

*IAN-CNR, v. Ferrata 1, 27100 Pavia (Italy)
†ICIST-IST,DECivil, Av. Rovisco Pais, 1049-001 Lisbon (Portugal)

The fundamental idea underlying such bases is that, in a multiscale analysis, the space V_j corresponding to a uniform discretization with step-size $h = 2^{-j}$, can be obtained as the span of two different bases. The nodal basis of scaling functions $\{\varphi_{jk}\}$ and the hierarchical basis of wavelets $\{\psi_{mk},\ m = j_0, \ldots, j-1\}$. Such a basis is obtained by decomposing V_j as $V_j = V_{j-1} \oplus W_{j-1} = V_{j_0} \oplus_{m=j_0}^{j-1} W_m$, where the *detail* or *complement spaces* W_m are defined as $W_m = (P_{m+1} - P_m)V_{m+1}$, $P_m : L^2(\mathbb{R}) \longrightarrow V_m$ being the L^2 orthogonal projection, or in the bi-orthogonal case an L^2 bounded projection operator. The change of basis between the two, can be performed by applying the Fast Wavelet Transform, which costs $O(2^j)$ operations.

It is important to underline the known fact that when expressing a function in V_j in terms of the nodal basis, generally, no matter how smooth it is, all the coefficients will be needed in order to get a good approximation, while, in expressing the same function in the wavelet basis, in order to get an approximation of the same order, one would usually need only a subset of the coefficients, (essentially the ones corresponding to those basis functions whose center is close to singularities).

In other words, the nodal basis naturally corresponds to taking a uniform discretization and the wavelet basis to a non uniform one.

There is however the problem of selecting a grid which is well suited to the solution of a given problem. This is usually done through the application of an adaptive scheme. Adaptive refinement based on different types of a posteriori error estimations has been studied recently in several papers [14, 27, 22]. In particular, wavelet based adaptive schemes have been studied in different papers and with different approaches [20, 8, 4, 26], which have in common the fact of taking advantage in one way or another of norm equivalence properties of the form (2.17). In the framework of Galerkin discretizations it is known that a hierarchical decomposition of the approximate solution provides an a posteriori error estimator ([1]). Although such a theory does not apply to collocation schemes, one can nevertheless try to apply the same principle also to such a case. In particular, in the framework of collocation with Deslaurier-Dubuc interpolating multiscale decomposition, the ideas of [20] have been tested on Burgers equation in [2].

The application of such techniques in the framework of the solution of linear elliptic PDEs, in dimension d, has been illustrated in [4]. This paper reports the application of the adaptive collocation techniques to the solution of plane elasticity problems. In section 2 the fundamental relations in elasticity are presented. In section 3, the adaptive collocation technique is described in detail. The numerical applications are presented and discussed in section 4. Three structures are analyzed to illustrate and characterize the application of this adaptive technique. The first numerical test is used to assess the accuracy and efficiency of the adaptive refinement procedure under analysis. The second example shows the capacity of such technique to detect and treat singularities in the stress field. Finally, the application of the algorithm to the analysis if non-rectangular structures is illustrated.

2 Fundamental relations

This paper illustrates the application of the adaptive collocation techniques based on the use of interpolating wavelets in the solution of plane elasticity problems. The field quantities involved in the description of the behavior of the structure depend on two coordinates only, assumed here as (x, y). The boundary conditions are imposed along a line $\Gamma(x, y) = 0$ lying on the same $xy-$ plane.

Two types of problems may arise in such conditions: the plain stress and plain strain problems [24, 3]. The plane stress state will occur when a thin plate is loaded by forces *living* in the plane $xy-$, applied both in the domain and on the boundary of the structure, but uniformly distributed over the thickness. A plane strain problem will appear when the dimension of the body in the z direction is very large when compared with its dimensions in the $xy-$ plane and the body is loaded by forces that are perpendicular to the longitudinal axis and remain constant along z. In these conditions, it is assumed that all cross sections (provided their distance from the end supports is enough) are in the same conditions.

The same field quantities are used to describe the behavior of both plane stress and plane strain problems. The equations relating those quantities are also the same, except for the case of the elasticity conditions [24], as described later.

The domain of the structure is denoted by Ω, while the boundary is represented by Γ. The boundary is subdivided into two parts. The first is usually known as *kinematic boundary*, Γ_u, and it is the portion of the enveloping surface where the value of the displacements are prescribed (Dirichlet boundary conditions). The part of the boundary where the loads are imposed (Neumann boundary conditions) is called usually *static boundary*, Γ_σ. It is important to stress that mixed boundary conditions may occur, as illustrated in figure 1, where $\Gamma_{\sigma\, u}$ represents part of the boundary where the displacements are imposed in one direction and the loads are prescribed in the other. For the sake of simplicity we will however make throughout this papee the assumption that $\Gamma_{\sigma\, u} = \emptyset$, though the method that we propose easily generalize to the case where $\Gamma_{\sigma\, u} \neq \emptyset$

In figure 1, vectors $\mathbf{b}$ and $\mathbf{t}_\gamma$ represent the loads applied in the domain and on the

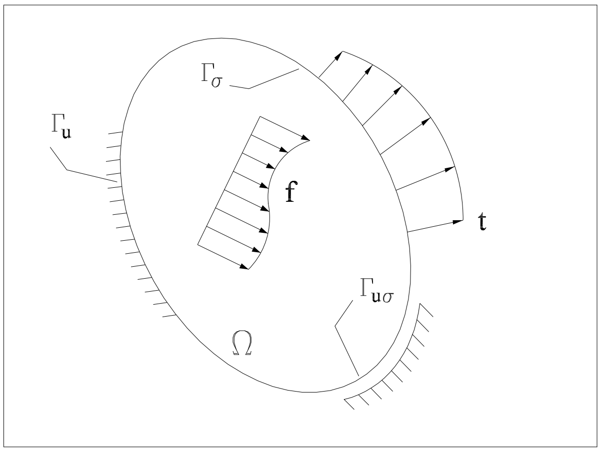

Figure 1: *Plane elasticity problem*

static boundary of the plate, respectively.

$$\mathbf{b} = \left\{ \begin{array}{c} b_x \\ b_y \end{array} \right\} \;, \; \mathbf{t} = \left\{ \begin{array}{c} t_{x\gamma} \\ t_{y\gamma} \end{array} \right\} \;.$$

Given the geometry of the structure, the elastic characteristics of the material, and the loads applied both in the domain and on the boundary, the fundamental problem of elasticity consists in the computation of all physical quantities necessary for the characterization of the behavior of the structure. These quantities are the displacements, the strains and the stresses. From an engineering point of view, the most important information for the design process is the accurate knowledge of the stress field.

To completely characterize the final location of each point of the structure, it is necessary to define the two independent components of the displacement vector field, u_x and u_y. The deformation of the elastic body is completely defined by the second order strain tensor, ε_{ij}. The independent components of this tensor may be listed in the vector:

$$\boldsymbol{\varepsilon} = \left\{ \begin{array}{c} \varepsilon_{xx} \\ \varepsilon_{yy} \\ \varepsilon_{xy} \end{array} \right\}$$

The two first components of vector ε represent the elongation along the x and y direction, respectively. The distortion of the structure is defined by the value of ε_{xy}. In structural mechanics, this value is usually replaced in the analysis by the total distortion parameter, $\gamma_{xy} = 2\ \varepsilon_{xy}$. In the plain strain problems it is assumed that $\varepsilon_{zz} = \varepsilon_{zx} = \varepsilon_{zy} = 0$.

The distribution of the stresses in the structure is characterized by a second order tensor, σ_{ij}. The independent components of this tensor may also be listed in a vector

$$\boldsymbol{\sigma} = \left\{ \begin{array}{c} \sigma_{xx} \\ \sigma_{yy} \\ \sigma_{xy} \end{array} \right\}$$

The two first components of $\boldsymbol{\sigma}$ correspond to the normal stresses acting on planes normal to the x and y axes, respectively. The shear stress field is denoted by σ_{xy}. In a plain stress problem it is assumed that $\sigma_{zz} = \sigma_{zx} = \sigma_{zy} = 0$.

In structural mechanics, the equations involving the kinematic quantities (displacements and strains) are known as *compatibility conditions*. These conditions in the domain relate the strains and the independent displacement fields as follows:

$$\varepsilon_x = \frac{\partial u_x}{\partial x} \tag{1}$$

$$\varepsilon_y = \frac{\partial u_y}{\partial y} \tag{2}$$

$$\gamma_{xy} = \frac{\partial u_x}{\partial y} + \frac{\partial u_y}{\partial x} \tag{3}$$

The kinematic (Dirichlet) boundary conditions may be written as

$$u_x = \overline{u}_x \quad on \quad \Gamma_u \tag{4}$$

$$u_y = \overline{u}_y \quad on \quad \Gamma_u \tag{5}$$

where $\overline{u}_x$ and $\overline{u}_y$ denote the known values of the displacements on that portion of the boundary.

The *elasticity conditions* relate the independent components of the stress and strain tensors. For plane stress problems, it is possible to write:

$$\sigma_{xx} = \frac{E}{1-\nu^2}\,(\varepsilon_x + \nu\varepsilon_y) \tag{6}$$

$$\sigma_{yy} = \frac{E}{1-\nu^2}\,(\nu\,\varepsilon_x + \varepsilon_y) \tag{7}$$

$$\sigma_{xy} = \frac{E}{2\,(1+\nu)}\,\gamma_{xy} \tag{8}$$

In equations (6), (7) and (8), parameters E and ν define the elastic properties of an homogeneous, isotropic material. They correspond to the Young modulus and to the Poisson ratio, respectively.

These elasticity relations have to be modified to allow for the consideration of plane strain problems [24]. However, the same equations may be used if the real elastic parameters are redefined according to the following expressions [3]:

$$E' = \frac{E}{1-\nu^2} \qquad \nu' = \frac{\nu}{1-\nu}$$

The static variables (stresses and applied loads) have to satisfy, both in the domain and on the static boundary, the so called *equilibrium conditions*. In Ω, these conditions are expressed as follows:

$$\frac{\partial\,\sigma_{xx}}{\partial\,x} + \frac{\partial\,\sigma_{xy}}{\partial\,y} + f_x = 0 \tag{9}$$

$$\frac{\partial\,\sigma_{xy}}{\partial\,x} + \frac{\partial\,\sigma_{yy}}{\partial\,y} + f_y = 0 \tag{10}$$

The static (Neumann) boundary conditions correspond to

$$\sigma_{xx}\,n_x + \sigma_{xy}\,n_y = \bar{t}_x \tag{11}$$

$$\sigma_{xy}\,n_x + \sigma_{yy}\,n_y = \bar{t}_y \tag{12}$$

To express the stresses in terms of the components of the displacement field, it is necessary to replace the compatibility relations into the elasticity conditions. It is then possible to write

$$\sigma_{xx} = e_1\,\frac{\partial\,u_x}{\partial\,x} + e_2\,\frac{\partial\,u_y}{\partial\,y} \tag{13}$$

$$\sigma_{yy} = e_2\,\frac{\partial\,u_x}{\partial\,x} + e_1\,\frac{\partial\,u_y}{\partial\,y} \tag{14}$$

$$\sigma_{xy} = e_3\left(\frac{\partial u_x}{\partial y} + \frac{\partial u_y}{\partial x}\right) \tag{15}$$

where the parameters e_1, e_2 and e_3 are computed using the values specified for the Young modulus and Poisson ratio.

$$e_1 = \frac{E}{1-\nu^2} \tag{16}$$

$$e_2 = \frac{\nu\,E}{1-\nu^2} \tag{17}$$

$$e_3 = \frac{E}{2\,(1+\nu)} \tag{18}$$

To obtain the system of differential equations that rules the behavior of the structure, it is necessary to replace equations (13)-(14) into the equilibrium conditions (9)-(10). This leads to the following system

$$\begin{bmatrix} e_1 \dfrac{\partial^2}{\partial x^2} + e_3 \dfrac{\partial^2}{\partial y^2} & (e_2 + e_3) \dfrac{\partial^2}{\partial x \, \partial y} \\ (e_2 + e_3) \dfrac{\partial^2}{\partial x \, \partial y} & e_2 \dfrac{\partial^2}{\partial x^2} + e_1 \dfrac{\partial^2}{\partial y^2} \end{bmatrix} \begin{bmatrix} u_x \\ u_y \end{bmatrix} + \begin{bmatrix} f_x \\ f_y \end{bmatrix} = \begin{bmatrix} 0 \\ 0 \end{bmatrix} \tag{19}$$

The static boundary conditions may be also expressed in terms of the displacements, yielding the following expressions:

$$\begin{bmatrix} e_1 \, n_x \dfrac{\partial}{\partial x} + e_3 \, n_y \dfrac{\partial}{\partial y} & e_2 \, n_x \dfrac{\partial}{\partial y} + e_3 \, n_y \dfrac{\partial}{\partial x} \\ e_3 \, n_x \dfrac{\partial}{\partial y} + e_2 \, n_y \dfrac{\partial}{\partial x} & e_3 \, n_x \dfrac{\partial}{\partial x} + e_1 \, n_y \dfrac{\partial}{\partial y} \end{bmatrix} \begin{bmatrix} u_x \\ u_y \end{bmatrix} = \begin{bmatrix} t_x \\ t_y \end{bmatrix} \tag{20}$$

where n_x and n_y denote the components of the unit outward normal associated with the considered boundary. For the sake of simplicity we will in the following introduce the notation

$$\mathcal{A} = \begin{bmatrix} e_1 \dfrac{\partial^2}{\partial x^2} + e_3 \dfrac{\partial^2}{\partial y^2} & (e_2 + e_3) \dfrac{\partial^2}{\partial x \, \partial y} \\ (e_2 + e_3) \dfrac{\partial^2}{\partial x \, \partial y} & e_2 \dfrac{\partial^2}{\partial x^2} + e_1 \dfrac{\partial^2}{\partial y^2} \end{bmatrix}, \qquad \mathbf{f} = - \begin{bmatrix} f_x \\ f_y \end{bmatrix}$$

$$\mathcal{B} = \begin{bmatrix} e_1 \, n_x \dfrac{\partial}{\partial x} + e_3 \, n_y \dfrac{\partial}{\partial y} & e_2 \, n_x \dfrac{\partial}{\partial y} + e_3 \, n_y \dfrac{\partial}{\partial x} \\ e_3 \, n_x \dfrac{\partial}{\partial y} + e_2 \, n_y \dfrac{\partial}{\partial x} & e_3 \, n_x \dfrac{\partial}{\partial x} + e_1 \, n_y \dfrac{\partial}{\partial y} \end{bmatrix}, \qquad \mathbf{t} = \begin{bmatrix} t_x \\ t_y \end{bmatrix}$$

so that we can write the problem as follows

Problem 2.1 *A Find* $\mathbf{u} = [u_x, u_y]^T$ *such that*

$$\begin{cases} \mathcal{A}\mathbf{u} = \mathbf{f} & in \ \Omega \\ \mathbf{u} = \mathbf{g} & on \ \Gamma_u \\ \mathcal{B}\mathbf{u} = \mathbf{t} & on \Gamma_\sigma . \end{cases}$$

3 The Adaptive Collocation Method

3.1 Interpolating MRA and Interpolating Wavelets

This section is devoted to recalling some properties of the the multiresolution framework in which the method will be stated. In the following we will denote by $\|\cdot\|_{s,p,\Omega}$ the $W^{s,p}(\Omega)$ norm, and by $\|\cdot\|_{s,\Omega}$ the $H^s(\Omega)$ norm.

Let φ_L be the Daubechies compactly supported scaling function of order L, [10]. The function φ_L satisfies, among other properties,

(i) $supp\, \varphi_L = [0, 2L+1]$.

(ii) $\varphi_L \in W^{R/2,\infty}$ for some $R > 0$ (R is proportional to L): $|(d^s/dx^s)\varphi_L| \leq C$, for all integer s $0 \leq s \leq R/2$;

(iii) φ_L satisfies a two-scale relation (the "refinement equation") which in the Fourier domain takes the form

$$\widehat{\varphi_L}(\xi) = m_0(\xi/2)\widehat{\varphi_L}(\xi/2),$$

(m_0 is a trigonometric polynomial of degree $2L+1$);

(iv) φ_L is orthogonal to its integer translates: $\int \varphi_L(x)\varphi_L(x-k)\, dx = \delta_{0k}$

(v) Polynomials up to order L can be written as a linear combination of the integer translates of φ_L.

The *Deslaurier-Dubuc fundamental function* ϑ of order $N = 2L+1$, is defined as the autocorrelation of φ_L:

$$\vartheta(x) = \int_{\mathbb{R}} \varphi_L(y)\varphi_L(y-x)\, dy.$$

As a consequence of (i-v) the function ϑ satisfies the following properties:

1) $supp\, \vartheta = [-N, N]$, and $\vartheta \in W^{R,\infty}$;

2) the function ϑ clearly satisfies itself a two scale relation. In fact it satisfies $\widehat{\vartheta} = |\widehat{\varphi}_L|^2$, and hence (2.1) gives

$$\widehat{\vartheta}(\xi) = |m_0(\xi/2)|^2\widehat{\vartheta}(\xi/2).$$

3) As a direct consequence of the orthogonality of the translates of φ_L the function ϑ satisfies the following interpolation property:

$$\vartheta(n) = \int_{\mathbb{R}} \varphi_L(y)\varphi_L(y-n)\,dy = \delta_{n0}.$$

4) As a consequence of (v), polynomials up to order N can be written as linear combinations of the integer translates of ϑ.

Remark 3.1 *The function ϑ was originally introduced by G. Deslaurier and S. Dubuc [11] as the limit function of an interpolatory subdivision scheme. Its relation with the minimal phase Daubechies orthonormal scaling functions was pointed out by G. Beylkin and N. Saito ([7]).*

Based on such a function we can easily build multiscale decompositions on $\mathbb{R}$ and, by tensor product, on $\mathbb{R}^d$.

In order to construct multiscale decomposition on the interval $]0,1[$ for $j \geq j_0 = [\log_2(N/2)] + 1$ (where $[\cdot]$ stands for the integer part) we define the interpolating basis functions on the interval by applying to the Deslaurier Dubuc functions the ideas of [CDV93, 12]. More precisely we let

$$\begin{aligned}
\vartheta_{jk} &= \vartheta(2^j x - k) + \sum_{n=-N+1}^{-1} a_{nk}\vartheta(2^j x - n), \qquad k = 0,..,L &(21)\\
\vartheta_{jk} &= \vartheta(2^j x - k), \qquad k = L+1, ..., 2^j - L - 1, &(22)\\
\vartheta_{jk} &= \vartheta(2^j x - k) + \sum_{n=2^j+1}^{2^j+N-1} b_{nk}\vartheta(2^j x - n), \qquad k = 2^j - L, .., 2^j, &(23)
\end{aligned}$$

with extrapolation weights a_{nk} and b_{nk} defined by:

$$a_{nk} = l^1_{jk}(n2^{-j}), \qquad b_{nk} = l^2_{jk}(n2^{-j}),$$

where l^1_{jk} and l^2_{jk} denote the Lagrange interpolation polynomials of degree L defined respectively as

$$l^1_{jk} = \prod_{\substack{i=0\\ i\neq k}}^{L} \frac{x - i2^{-j}}{k2^{-j} - i2^{-j}}, \qquad l^2_{jk} = \prod_{\substack{i=2^j-L\\ i\neq k}}^{2^j} \frac{x - i2^{-j}}{k2^{-j} - i2^{-j}}.$$

Remark that a_{nk} and b_{nk} are indeed independent of j.

A multiresolution $\{V_j\}_{j\geq j_0}$ of $]0,1[$ is then defined as

$$V_j = span < \vartheta_{jk}, \quad k = 0,..,2^j > \subset \; L^2(0,1).$$

By tensor product we the easily define a multiresolution on the square: introducing the two dimensional scaling functions $\vartheta_{j,\mathbf{k}}, \;\; \mathbf{k} = (k_1, k_2) \in G_j = \{0,..,2^j\}^2$ defined as

$$\vartheta_{j,\mathbf{k}} = \vartheta_{jk_1} \otimes \vartheta_{jk_2}$$

we set

$$\mathbb{V}_j = span < \vartheta_{j,\mathbf{k}}, \;\; \mathbf{k} = (k_1, k_2) \in G_j >$$

It is immediate to define an interpolation operator $L_j : C^0([0,1]^2) \to \mathbb{V}_j$

$$L_j f = \sum_{\mathbf{k}\in G_j} f(\mathbf{k}/2^j)\vartheta_{j,\mathbf{k}}.$$

The wavelet basis for the complement space

$$\mathbb{W}_j = (L_{j+1} - L_j)\mathbb{V}_{j+1}$$

is composed by the functions

$$\psi_{j,\mathbf{k}}^{(1,0)} = \vartheta_{j+1,2k_1-1} \otimes \vartheta_{j,2k_2} \tag{24}$$

$$\psi_{j,\mathbf{k}}^{(0,1)} = \vartheta_{j,2k_1} \otimes \vartheta_{j+1,2k_2-1} \tag{25}$$

$$\psi_{j,\mathbf{k}}^{(1,1)} = \vartheta_{j+1,2k_1-1} \otimes \vartheta_{j+1,2k_2-1} \tag{26}$$

The grid-points corresponding to the scaling functions and the wavelets respectively will be indicated as

$$\zeta_{j,\mathbf{k}} = (k_1 2^{-j}, k_2 2^{-j}), \qquad \xi_{j,\mathbf{k}}^{(1,0)} = ((2k_1-1)2^{-(j+1)}, k_2 2^{-j}),$$

$$\xi_{j,\mathbf{k}}^{(0,1)} = (k_1 2^{-j}, (2k_2-1)2^{-(j+1)}), \qquad \xi_{j,\mathbf{k}}^{(1,1)} = ((2k_1-1)2^{-(j+1)}, (2k_2-1)2^{-(j+1)}).$$

In the following it will be practical to introduce the following compact notation on the indexes: given $\lambda = (\eta, j, \mathbf{k})$ with $\eta \in \Xi = \{0,1\}^2 \backslash \{0,0\}$, $j \geq j_0$, and $\mathbf{k}$ such that $\xi_{j,\mathbf{k}}^\eta \in [0,1]^2$, we set

$$\psi_\lambda = \psi_{j,\mathbf{k}}^\eta, \qquad\qquad \xi_\lambda = \xi_{j,\mathbf{k}}^\eta.$$

Each continuous function $f \in C^0([0,1]^2)$ can be expanded as

$$f = \sum_{\mathbf{k}\in\{0,..,2^{j_0}\}^2} \beta_{j_0\mathbf{k}} \vartheta_{j_0\mathbf{k}} + \sum_{\lambda\in\Lambda} \alpha_\lambda \psi_\lambda,$$

where

$$\Lambda = \{(\eta, j, \mathbf{k}),\ \eta \in \Xi, j \geq j_0, \mathbf{k} \text{ such that } \xi^\eta_{j,\mathbf{k}} \in [0,1]^2\}$$

denotes the set of compact indexes. For $j \geq j_0$ fixed, we set

$$\Lambda_j = \{(\eta, j, \mathbf{k}),\ \eta \in \Xi, \mathbf{k} \text{ such that } \xi^\eta_{j,\mathbf{k}} \in [0,1]^2\}$$

so that $\Lambda = \cup_{j\geq j_0} \Lambda_j$.

Remark that if a dyadic point $p = (\mathbf{n})/2^m \in [0,1]^2$ verifies $p \notin \{\zeta_{j_0,\mathbf{k}},\ \mathbf{k} \in G_{j_0}\}$, then there exists a unique $\lambda(p)$ such that

$$p = \frac{\mathbf{n}}{2^m} \longrightarrow \lambda(p) \in \Lambda : \qquad p = \xi_{\lambda(p)}. \tag{27}$$

The spaces $\mathbb{V}_j$ satisfy a Strang-Fix condition of order N, which implies that the following approximation property holds: if $f \in H^s(]0,1[^2)$, $1 < s \leq N+1$ then $\forall r \leq s$, $0 \leq r \leq R$ we have

$$\|f - L_j f\|_{r,]0,1[^2} \leq C 2^{-j(s-r)} \|f\|_{s,]0,1[^2}.$$

Such a multiscale decomposition has been extensively investigated in [12], where several properties which will play an important role in the following have been stated. In particular we recall that it is possible to define an *interpolating wavelet transform* mapping any continuous function f into the sequence of coefficients

$$\mathbf{w}(f) = \{\{\beta_{j_0,\mathbf{n}},\ \mathbf{n} \in G_{j_0}\}, \{\alpha_\lambda, \lambda \in \Lambda\}\},$$

defined as

$$\beta_{j_0,\mathbf{n}} = f(\zeta_{j_0,\mathbf{n}}), \qquad \text{and for } \lambda \in \Lambda_j, \qquad \alpha_\lambda = f(\xi_\lambda) - L_j f(\xi_\lambda). \tag{28}$$

Formula (28) clearly shows that the wavelet coefficients α_{jk} measure the lack of approximation of f by $L_j f$ at the point ξ_λ. In fact, a stronger result holds. It is possible to prove ([12, 13]) that the result of characterization of Besov spaces that holds for orthonormal wavelets, carries on to interpolating wavelets on $(0,1)$, provided that the Besov space considered is embedded in $C^0(0,1)$. In particular in dimension two this holds for the Sobolev spaces $H^s(0,1)$ provided $s > 1$. In other words, the size of the coefficients β_λ gives us information on eventual singularities in all the derivatives of a function f up to a certain order. This is a key point in the behavior of our method.

As in the usual framework of biorthogonal wavelets we have a *fast wavelet transform* algorithm, acting on functions in $\mathbb{V}_j$. Given the coordinates of a function $f \in \mathbb{V}_j$ with respect to the *scaling functions* basis $\{\vartheta_{j,\mathbf{n}}, \quad \mathbf{n} \in G_j\}$ the FWT provides the coordinates of f with respect to the wavelet basis $\{\vartheta_{j_0,\mathbf{n}}, \quad \mathbf{n} \in G_{j_0}\} \cup_{m=j_0}^{j-1} \{\psi_\lambda, \quad \lambda \in \Lambda_j\}$. However, unlike in the usual biorthogonal case, the coordinates with respect to the scaling function basis are nothing but the values of f at the dyadic points. Moreover, the matrix realizing such a change of basis turns out to be lower triangular. This plays an important role in the efficient implementation of the method [4, 6]

3.2 Collocation on Non-Uniform Grids

Let us now briefly recall how the above mentioned structure can be employed to design a collocation method on non uniform dyadic grids. For any finite subset $\Lambda_h \subset \Lambda$ of the index set Λ, we define a corresponding finite grid of dyadic points G_{Λ_h} as

$$G_{\Lambda_h} := \{\zeta_{j_0,\mathbf{k}}, \quad \mathbf{k} \in G_{j_0}\} \cup \{\xi_\lambda, \quad \lambda \in \Lambda_h\}.$$

(in order to have a minimum degree of approximation the grid G_h will be assumed to contain the coarse grid of mesh size 2^{-j_0}), and we will denote by

$$V_{\Lambda_h} = V_{j_0} \oplus span < \psi_\lambda, \lambda \in \Lambda_h >$$

the space spanned by the basis functions corresponding to the selected points.

It will also be convenient in the following to introduce the corresponding interpolation operator $L_{\Lambda_h} : C^0(\overline{\Omega}) \longrightarrow V_{\Lambda_h}$. Given $f \in C^0(\overline{\Omega})$, $L_{\Lambda_h} f \in V_{\Lambda_h}$ is the unique function satisfying

$$L_{\Lambda_h} f(p) = f(p) \quad \text{for all nodes } p \in G_h = G_{j_0} \cup \Lambda_h.$$

By abuse of notation, for $\mathbf{u} = (u_x, u_y) \in C^0(\overline{\Omega})^2$ we will denote by $L_{\Lambda_h}\mathbf{u}$ the vector $(L_{\Lambda_h} u_x, L_{\Lambda_h} u_y) \in V_{\Lambda_h}^2$.

In order to take into account boundary conditions the grid G_{Λ_h} is split as the union of the set of interior nodes and the set of respectively Neumann and Dirichlet boundary nodes:

$$G_{\Lambda_h} = G^{(i)}_{\Lambda_h} \cup G^{(N)}_{\Lambda_h} \cup G^{(D)}_{\Lambda_h} \tag{4.5}$$

with

$$G^{(i)}_{\Lambda_h} = G_{\Lambda_h} \cap]0,1[^2, \qquad G^{(N)}_{\Lambda_h} = G_{\Lambda_h} \cap \Gamma_\sigma, \qquad G^{(D)}_{\Lambda_h} = G_{\Lambda_h} \cap \Gamma_u. \tag{4.6}$$

Problem (P) can then be discretized as follows:

Problem 3.1 *B Given $\Lambda_h \subset \Lambda$, find $\mathbf{u} \in V_{\Lambda_h}$ such that*

$$\begin{cases} \mathcal{A}\mathbf{u}_h(p) = f(p) & \textit{for all nodes } p \in G^{(i)}_{\Lambda_h} \\ \mathbf{u}_h(p) = g(p) & \textit{for all nodes } p \in G^{(D)}_{\Lambda_h} \\ \mathcal{B}\mathbf{u}_h(p) = \mathbf{t}(p) & \textit{for all nodes } p \in G^{(N)}_{h} \end{cases}$$

3.3 The adaptive collocation scheme

We can now briefly describe the adaptive collocation scheme proposed in [4]. The idea is to iteratively compute increasingly good approximations to the solution $\mathbf{u}$ of Problem 1. and use the actual approximate solution at each iteration in order to design a better grid to be used for computing the next approximate solution.

We select the first grid $G^0_h = G_{\Lambda_0}$ by requiring that the right hand side $\mathbf{f}$ is well approximated on such grid, in the sense that

$$\|\mathbf{f} - L_{\Lambda_0}\mathbf{f}\|_{t,\infty} \leq \varepsilon. \tag{5.1}$$

Once the first grid G^0 has been selected, compute a first approximate solution u_0 by applying a collocation method in the corresponding space $U_0 = V_{\Lambda_0}$, according to the formulation (3.1).

Following the idea of [20, 26, 6, 4], we then analyze the computed solution in order to design a new (better) grid. More precisely, at the $n-$th step, given a grid G^n, and the relative approximate solution $\mathbf{u}_n$ with coefficients

$$\mathbf{w}(u^n_x) = \{\{c^{x,n}_{j_0,\mathbf{k}}\}, \{e^{x,n}_\lambda,\ \lambda \in \Lambda_n\}\}, \qquad \mathbf{w}(u^n_y) = \{\{c^{y,n}_{j_0,\mathbf{k}}\}, \{e^{y,n}_\lambda,\ \lambda \in \Lambda_n\}\}$$

we compute the next grid G^{n+1} by removing the useless points and refining where the approximation is bad. For each point ξ_μ, $\mu = (\eta, j, \mathbf{k})$, $\eta \in \Xi$, $j \geq j_0$, $\mathbf{k} \in \{1, \cdots, 2^j\}^2$, define a set U_μ of neighboring points

$$U_\mu = [0,1]^2 \cap \{\zeta_k^{j+1}, \quad k = (2k_1 + \eta_1, \ldots, 2k_d + \eta_d), \quad \eta_i = -1, 0, 1\},$$

and the corresponding index set $\mathcal{U}_\mu$ as

$$\mathcal{U}_\mu = \{\lambda(p), \quad p \in U_\mu\}$$

(where, for a dyadic point p, $\lambda(p)$ is defined by (27)). Define then a set Λ_n^{sel} of indexes selected for refinement as

$$\Lambda_n^{sel} = \{\lambda : \ \max\{|e_\lambda^{x,n}|, |e_\lambda^{y,n}| > \delta_a/2^{js}\}.$$

We then introduce an updated index set

$$\Lambda_{n+1} = \{\lambda : \max\{|e_\lambda^{x,n}|, |e_\lambda^{y,n}|\} > \delta_r/(2^{js}j^2)\} \cup_{\mu \in \Lambda_n^{sel}} \mathcal{U}_\mu,$$

and the corresponding refined grid

$$G^{n+1} = G_{\Lambda_{n+1}}.$$

The $(n+1) - th$ approximation space is defined as

$$U_{n+1} = V_{\Lambda_{n+1}}.$$

The $(n+1)-$th approximate solution is computed by solving the collocation Problem B. on the space U^{n+1}, with collocation grid G^{n+1}.

We want to remark that one of the strength of the proposed refining procedure is its extreme simplicity. In particular it does not need extra computation of any quantities, the coefficient of the approximate solution themselves being the parameters driving the decision on whether to refine or not. Moreover, since the discretization is not based on any triangulation, adding or removing each point has no influence on the other points of the grid, since there is no conformity requirement to fulfill, which causes some difficulty when refining and derefining a finite element triangulation.

4 Numerical applications

The structures represented in figures 2, 3 and 4 are used to illustrate the use of the interpolant wavelets in the solution of structural engineering problems. It is assumed that these examples correspond to plane stress problems. It is always assumed also a physically and geometrically linear behavior.

First, the square cantilever plate subjected to a uniform load acting on its upper edge is used to illustrate the use of uniform grids. The solutions obtained are compared with the ones resulting from the application of other numerical techniques. The same structure is then used to show how efficient may be the use of the adaptive procedure described in the previous sections.

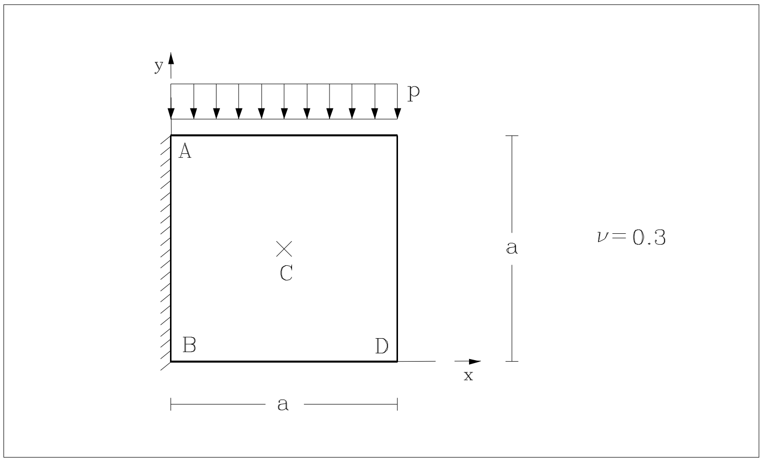

Figure 2: *Square cantilever plate*

The analysis of the square plate with a the central crack represented in figure 3 will show that the techniques being tested are quite effective in what concerns the detection and treatment of singularities existing in the stress field. It shows also that the use of non-uniform grids and adaptive refinement procedures leads to accurate numerical solutions with a relatively small number of degrees of freedom.

The analysis of the very simple gravity dam presented in figure 4 is used to illustrated the solution of problems defined over non-rectangular domains.

4.1 Analysis of the cantilever plate with uniform grids

Three different discretizations are used in the analysis of the square cantilever plate. In each of them, a uniform grid is considered with $N = 4$ and $j_0 = 3$. The different discretizations take increasing values for parameter j_{max}. Table 1 lists the characteristics of all discretizations, including the number of grid point in the mesh, n_{grid}, the total number of degrees of freedom, n_{dof} and the CPU time (in seconds), T_{CPU}, involved in the analysis. It must be stressed that this value does not include the

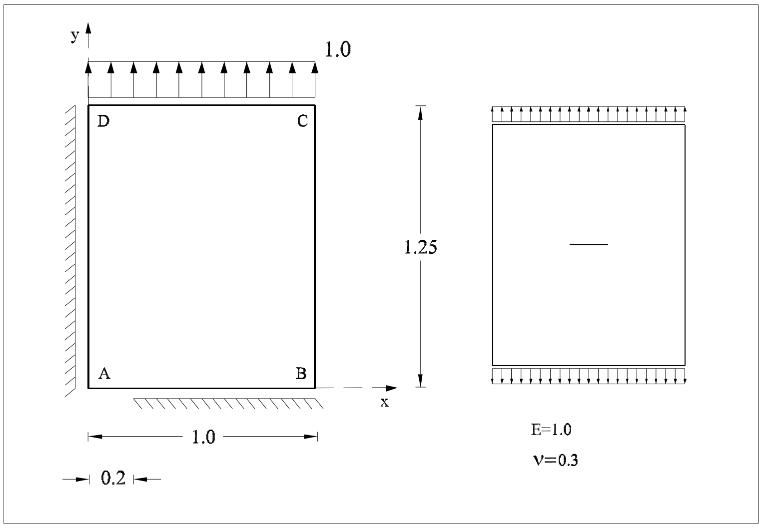

Figure 3: *Rectangular plate with a central crack*

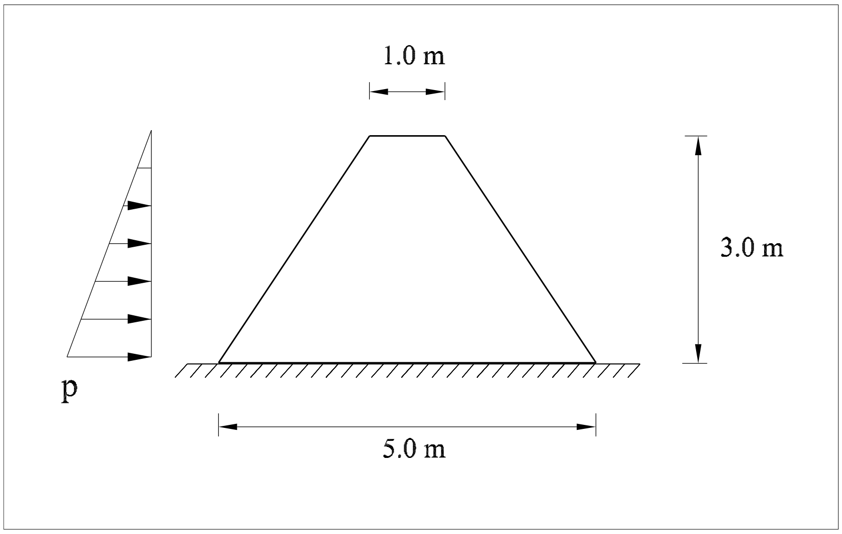

Figure 4: *Gravity dam*

time required by post-processing operations, as it will be discussed later. The examples presented in this paper were run on machine with an AMD Atlhon processor running Linux.

Discretization	N	j_0	j_{max}	n_{grid}	n_{dof}	T_{CPU}
A	4	3	3	81	162	0.04
B	4	3	4	289	578	0.72
C	4	3	5	1089	2178	52.63

Table 1: Discretizations involved in the analysis of the square cantilever

Figure 5 shows the solution obtained with discretization A. The three stress fields and the displacement field are plotted using the graphic routine package *Janela* [19]. For the representation of the stress fields, a finer uniform grid has been used. Each independent component of the stress tensor is then plotted in a grid of 65×65 dyadic points in the domain. It is important to remind clearly that this fine grid is used only to support the graphical representation of the solution; it is never used in the computations.

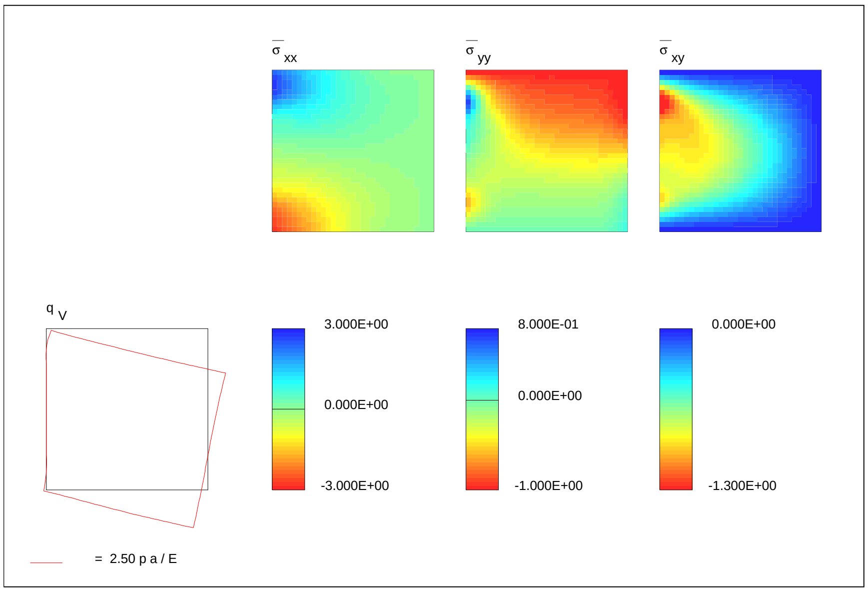

Figure 5: *Square cantilever plate; solution with discretisation A*

The solution represented in figure 6 was obtained using a commercial finite element code, COSMOS/M [9]. To obtain that solution, a mesh with 900 4-node bilinear elements was used, yielding a total of 1860 degrees of freedom. The stress field

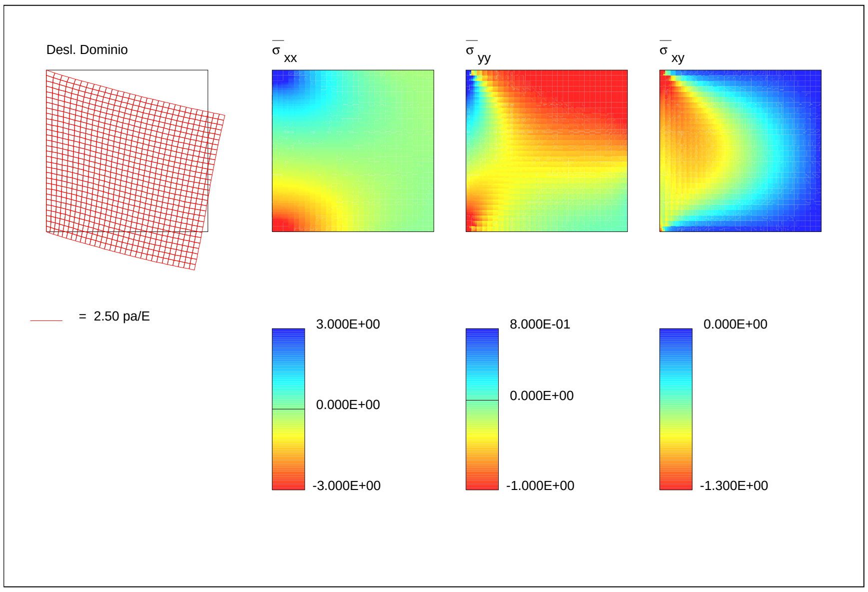

Figure 6: *Square cantilever plate; solution with finite elements*

is represented as it results directly from the computations without the use of any smoothing techniques. Comparing figures 5 and 6 it is possible to observe qualitatively that the use of interpolating wavelets leads to accurate solutions with a small number of degrees of freedom when compared to the classical displacement finite element model.

The accuracy of the solutions obtained is illustrated in tables 2 and 3. Table 2 shows the values computed for the components of the displacement field at point D (see figure 2).

	A	*B*	*B*	*Walsh*	*Daub*	*Mix_F*	*Mix_L*	*COSMOS*
$\overline{d}_x$	-1.114	-1.057	-1.044	-1.021	-1.042	-1.036	-1.041	-1.039
$\overline{d}_y$	-2.930	-2.941	-2.963	-2.970	-2.991	-2.981	-2.988	-2.979

Table 2: *Components of displacement field at point D.*

The values presented in table 2 are normalized according to:

$$\overline{d}_x = \frac{E}{p\,a} d_x \; ; \; \overline{d}_y = \frac{E}{p\,a} d_y$$

The same table lists also the values obtained with the alternative non-conventional hybrid-mixed stress finite element formulations [15, 16]. In these formulations, both the stresses and the displacements are independently approximated in each finite element. The displacements along the static boundary are also approximated. Apart from the kinematic boundary conditions, all the field equations are imposed in a weighted residual form so designed as to ensure that the discrete model embodies all relevant properties presented by the continuum model being discretized [17]. The model *Walsh* uses the orthonormal digital series introduced by JL Walsh [28] and the model *Daub* is based on the use of Daubechies [10] scaling functions. The solutions obtained with these models use a total of 59576 and 1644 degrees of freedom, respectively. The *Mix_F* and *Mix_L* models use as approximation bases the trigonometric functions [18] and the orthonormal Legendre polynomials [21] and the solutions presented in table 2 were obtained using 1544 and 1664 degrees of freedom, respectively.

Table 3 shows, for all test cases presented above, the values of the independent components of the stress tensor on the points A, B and C represented in figure 2. All values are normalized according to the rule:

$$\overline{\sigma}_{ij} = \frac{\sigma_{ij}}{p}$$

P		A	B	C	*Walsh*	*Wavelet*	*Mix_F*	*Mix_L*	*COSMOS*
A	$\overline{\sigma}_{xx}$	2.402	3.463	4.726	7.734	8.493	8.078	9.559	7.623
	$\overline{\sigma}_{yy}$	-1.000	-1.000	-1.000	-0.935	-0.998	-1.000	-1.000	2.287
	$\overline{\sigma}_{xy}$	0.000	0.000	0.000	-0.050	-0.001	0.000	0.000	-1.656
B	$\overline{\sigma}_{xx}$	-2.708	-3.295	0.029	-5.302	-5.391	-5.498	-6.237	-5.281
	$\overline{\sigma}_{yy}$	0.000	0.000	0.000	-0.037	0.000	0.000	0.000	-1.584
	$\overline{\sigma}_{xy}$	0.000	0.000	0.000	-0.018	0.000	0.000	0.000	-0.814
C	$\overline{\sigma}_{xx}$	0.026	0.029	0.031	0.031	0.031	0.036	0.028	0.031
	$\overline{\sigma}_{yy}$	-0.473	-0.472	-0.473	-0.474	-0.480	-0.476	-0.489	-0.473
	$\overline{\sigma}_{xy}$	-0.670	-0.716	-0.736	-0.747	-0.747	-0.745	-0.721	-0.747

Table 3: *Stresses on points A, B and C; equilibrated solution*

It is important to discuss the values obtained for the stresses on points A and B. The comparison of the results should not involve those points because it is known [3] that singularities will occur precisely there. However, when comparing the values listed in table 3, it is possible to verify that the solutions obtained with the interpolating wavelets lead to smaller stresses in the corners. This is due to the fact that on points A and B the Neumann boundary conditions are directly enforced in the collocation procedure, in order to fully satisfy the equilibrium along the boundary. In structural mechanics, it is always important to obtain *equilibrated* solutions. If the collocation scheme is changed in order to impose the Dirichlet boundary conditions on points A and B, the resulting stresses are closer to the finite element solutions, as illustrated in table 4 and the effect induced by the singularities is quite clear.

P		A	B	C	*COSMOS*
A	$\overline{\sigma}_{xx}$	8.387	10.588	13.180	7.623
	$\overline{\sigma}_{yy}$	2.516	3.176	3.954	2.287
	$\overline{\sigma}_{xy}$	-2.527	-3.009	-3.571	-1.656
B	$\overline{\sigma}_{xx}$	-5.934	-6.913	-8.088	-5.281
	$\overline{\sigma}_{yy}$	-1.780	-2.074	-2.426	-1.584
	$\overline{\sigma}_{xy}$	-1.357	-1.524	-1.753	-0.814
C	$\overline{\sigma}_{xx}$	0.027	0.029	0.031	0.031
	$\overline{\sigma}_{yy}$	-0.473	-0.472	-0.473	-0.473
	$\overline{\sigma}_{xy}$	-0.670	-0.716	-0.736	-0.747

Table 4: *Stresses on points A, B and C; compatible solution*

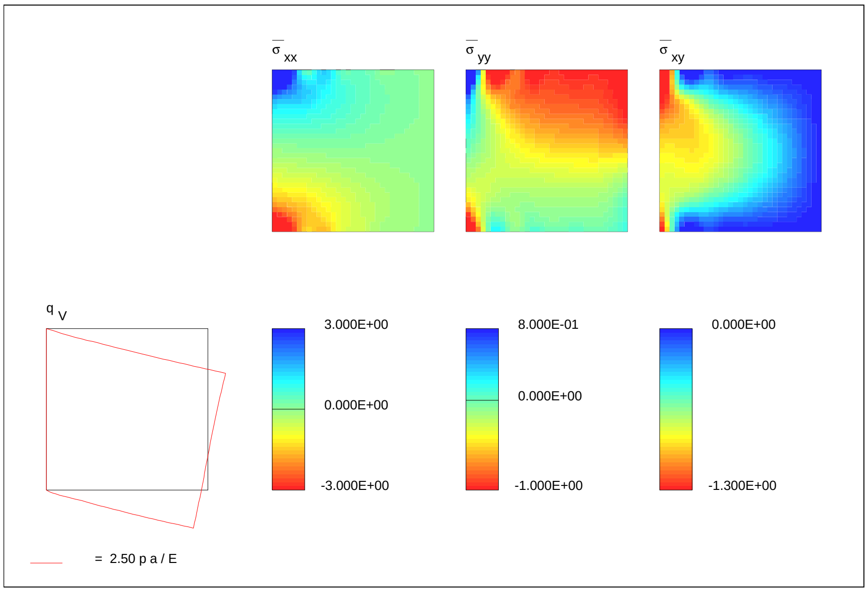

Figure 7: *Square cantilever plate; compatible solution with discretization A*

It is important to verify that the differences between the *compatible* and *equilibrated* solutions are concentrated around the corner points, as illustrated in figure 7. As expected, the differences tend to disappear if the degree of *resolution* is increased, as illustrated in figures 8 and 9. In both these situations, the solution involves the use of a uniform mesh but with $j_{max} = 5$.

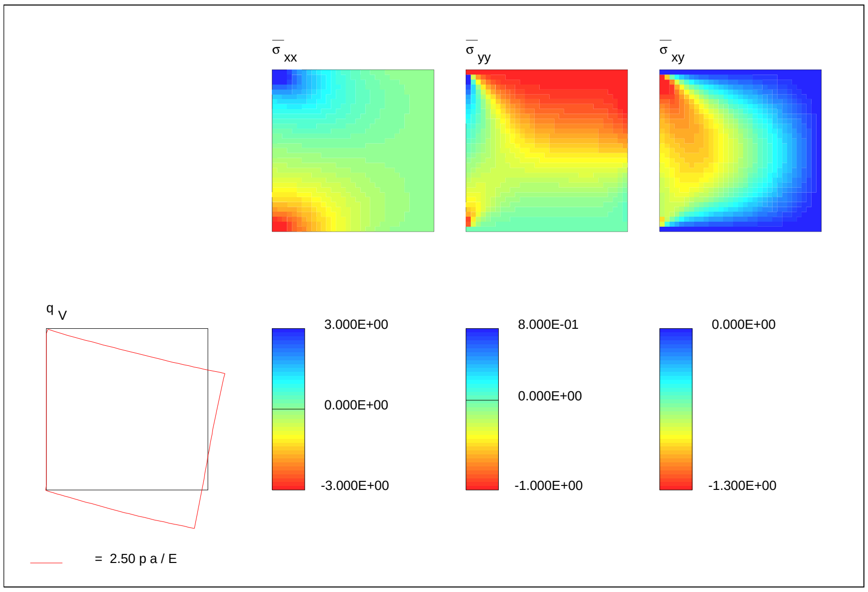

Figure 8: *Square cantilever plate; equilibrated solution with discretization C*

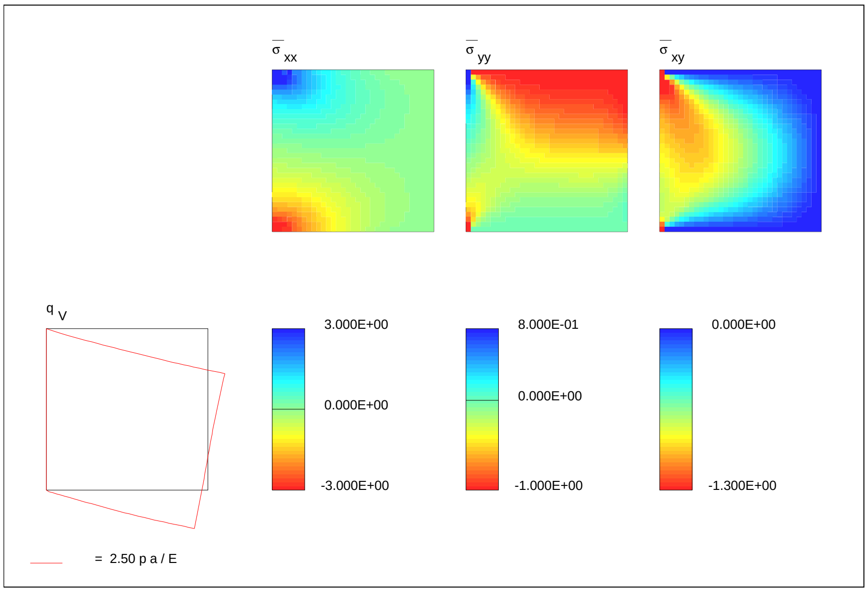

Figure 9: *Square cantilever plate; compatible solution with discretization C*

It is interesting to analyze the evolution of the strain energy with the number of degrees considered in the discretization. This information is presented in the graph included in figure 10. It shows that the energy converges to the exact solution as the number of grid points increases. The strain energy is defined by the following expression

$$U = \frac{1}{2} \int_V \sigma^t \, \varepsilon \, dV$$

For the computation of the strain energy error, it was assumed that its exact value is given by $U_{exact} = 0.9865$ [21]

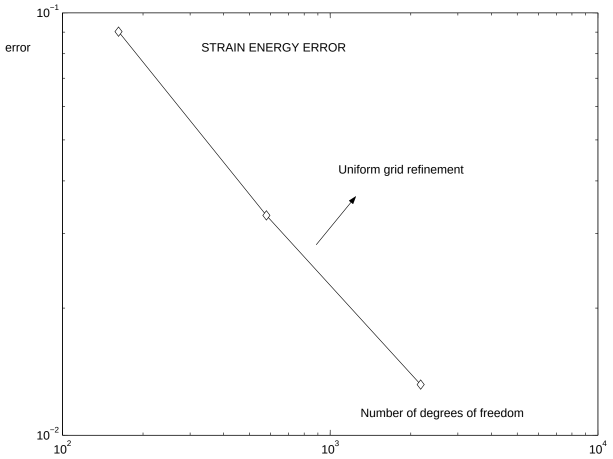

Figure 10: *Strain energy error evolution*

4.2 Analysis of the cantilever plate with non-uniform grids

In the previous section only uniform grids were considered in the analysis. However, this is not by far the most effective procedure to obtain an accurate solution for the problems being solved. To fully exploit the advantages of the collocation technique under analysis, a sequence of adaptive non-uniform grids should have been used.

To illustrate the application of an adaptive refinement procedure, lets take again the square cantilever plate shown in figure 2. Lets consider an initial uniform grid with $j_0 = 3$, $j_{max} = 4$ and $N = 4$. This initial mesh is the one represented at the top left corner of figure 11.

Then, the adaptive refinement procedure is applied using the following values for the parameters that control remeshing: $\delta_a = 1 \times 10^{-5}$ and $\delta_r = 1 \times 10^{-6}$. The sequence of non-uniform grids generated by the algorithm is presented also in figure 11. The final mesh is represented in its lower right corner. As expected, the grid points are concentrated mostly near the corners of the clamped edge, where the singularities of the stress field occurs.

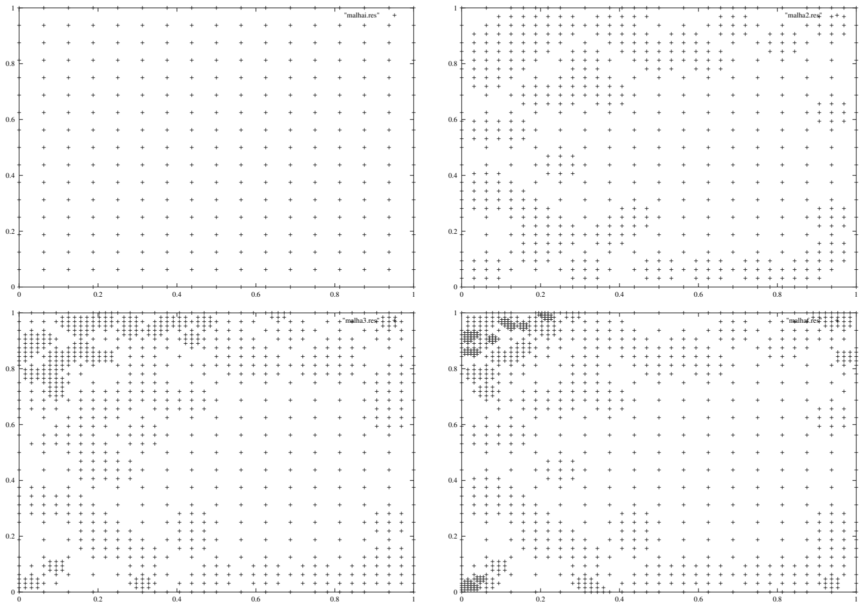

Figure 11: *Initial and final grids*

Mesh	j_{max}	n_{grid}	n_{dof}
initial	4	289	578
2	5	597	1194
3	6	868	1736
final	7	917	1834

Table 5: Adaptive non-uniform grids used in the solution of the square plate

Table 5 shows, for each grid, the number of points, n_{grid}, the number of degrees of freedom, n_{dof}, and the highest level of resolution, j_{max}. The final solution is computed in 12.50 seconds (except post-processing operations) and is represented in figure 12. It must be stressed that the accuracy of this solution is better than the accuracy of the uniform mesh with $j_{max} = 5$ and it is much more economic in terms of resources required for computation, both in terms of memory and CPU time.

This aspect is reinforced by the analysis of the plots in figure 13, where the evolution of the strain energy is presented for the uniform and non-uniform analysis presented before.

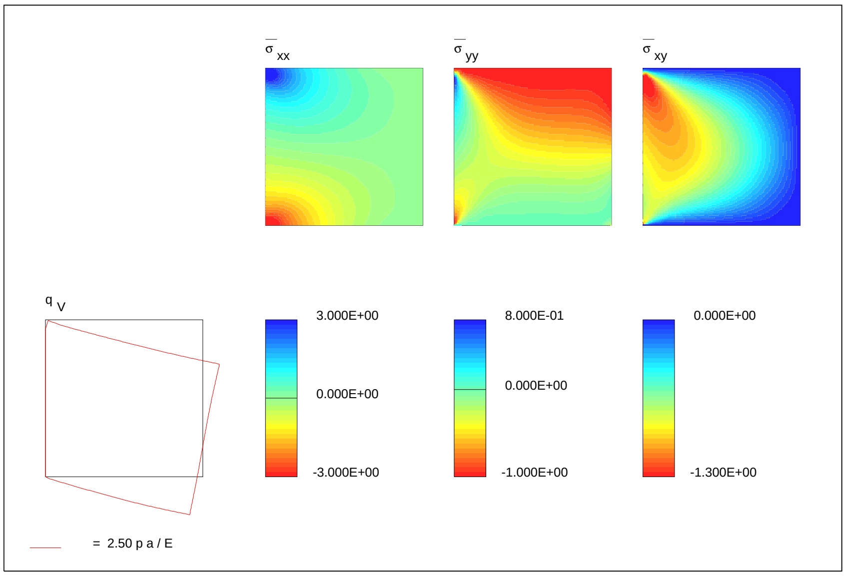

Figure 12: *Square cantilever plate; solution obtained with an adaptive refinement procedure*

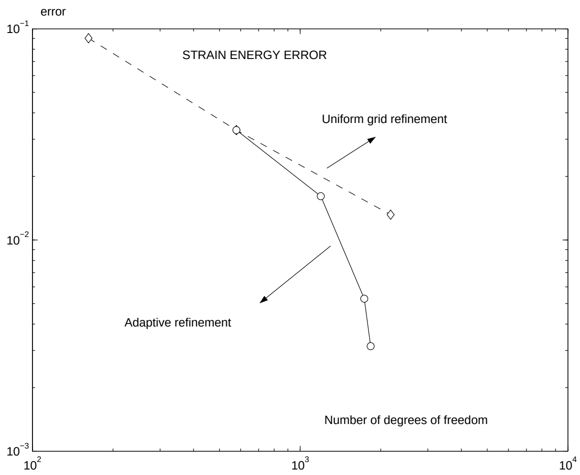

Figure 13: *Strain energy evolution for the uniform and non-uniform grids*

4.3 Analysis of the square plate with a central crack

The square plate with a central crack is a typical example where the use of an higher order scheme is highly recommended due to the existence of a strong singularity at the tip of the crack.

Due to symmetry, only one fourth of the structure is analyzed, as indicated in figure 3.

An adaptive collocation technique has been used to obtain an accurate solution with the smallest number of grid points. The initial solution taken corresponds to the use of a uniform grid with $j_0 = 2$, $j_{max} = 3$ and $N = 4$. This coarse mesh with only 81 degrees of freedom will lead to a coarse solution, as illustrated in figure 14.

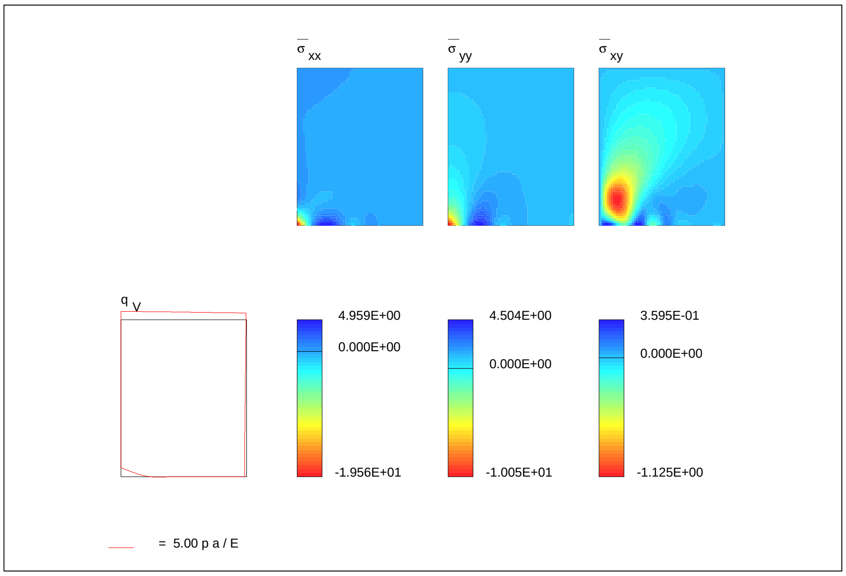

Figure 14: *Square plate with central crack; initial solution*

Applying the refinement procedure, the non-uniform grid presented in figure 15 is obtained after four remeshing procedures. It has 597 points, which means a total number of 1194 degrees of freedom. As expected, the grid points are concentrated around the crack.

The final solution is presented in figure 16. It is quite clear the quality of the solution obtained.

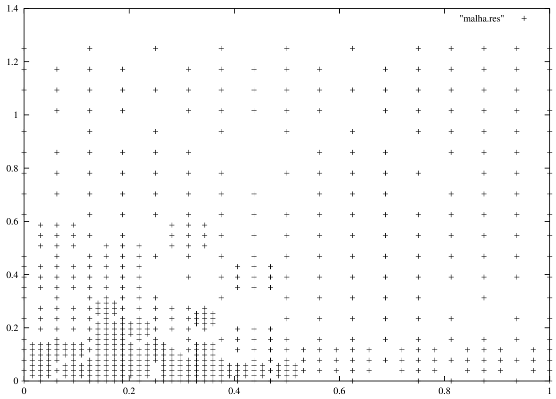

Figure 15: *Final non-uniform mesh in the analysis of the square plate with the central crack*

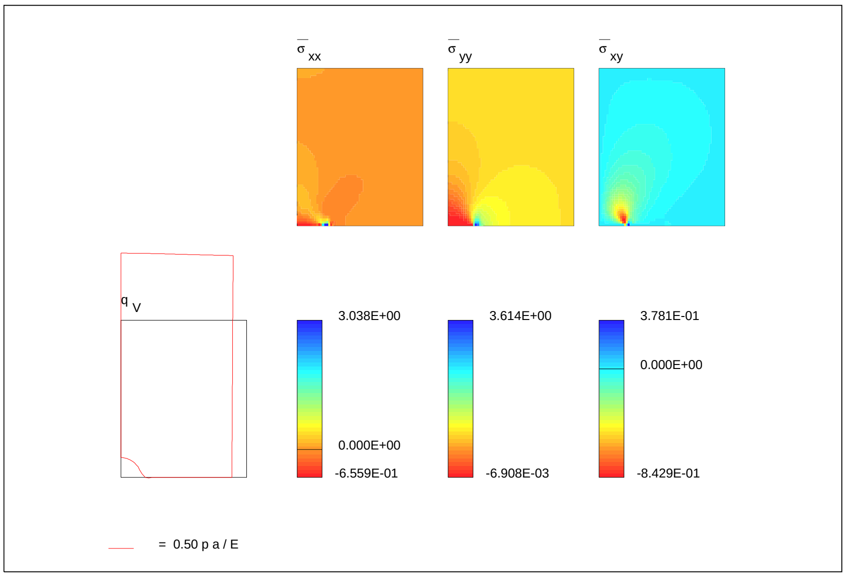

Figure 16: *Square plate with central crack; final solution*

4.4 Analysis of the gravity dam

The structure presented in figure 4 represents a gravity dam with a very simple geometry. As the computational domain is not rectangular, it must be mapped onto a unit square by means of a conformal mapping of class C^2 with a C^2 inverse, as explained in [4].

Three different static loading conditions have been tested. The first one considers only a triangular force, which is intended to model the water pressure acting on the dam. The second load corresponds to the self-weight of the material ($f_x = 0$ and $f_y = -25$). Finally, the third situation corresponds to the combination of the two previous loads.

In each case an initial uniform grid with 289 points was used. This grid corresponds to the use of parameters $j_0 = 3$, $j_{max} = 4$ and $N = 4$ and a total of 578 degrees of freedom. The elastic properties of the material are assumed to be characterized by the following parameters: $E = 1.0$ and $\nu = 0.3$.

The solutions for the three loading conditions are presented in figures 17, 19, and 21, respectively. These solutions were obtained with three adaptive refinement procedures. The final non-uniform grids are represented in figures 18, 20 and 22, respectively.

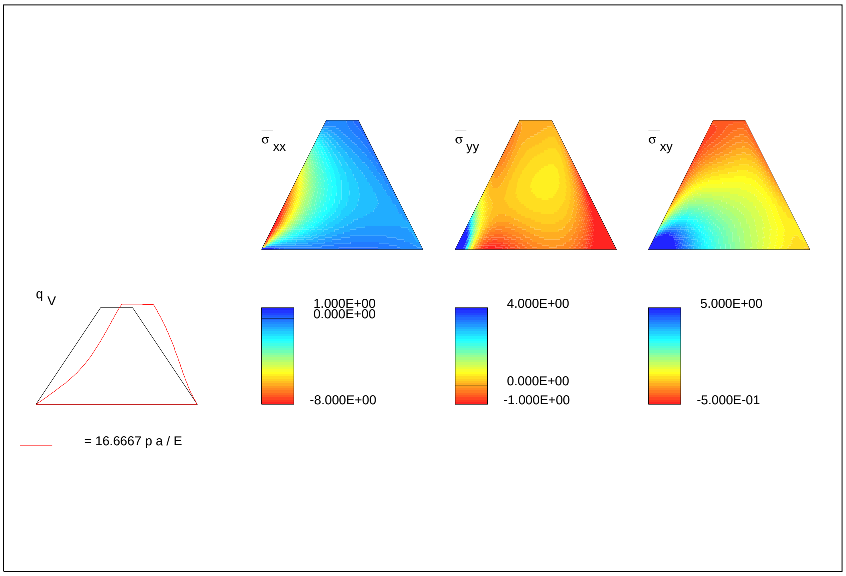

Figure 17: *Gravity dam with a triangular load applied*

Table 6 shows, for each load case, the number of grid points and the total number of

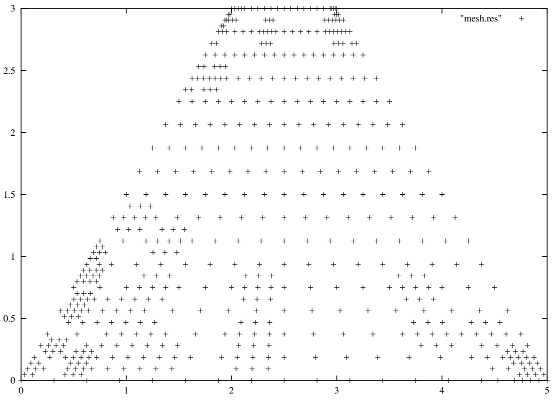

Figure 18: *Final non-uniform mesh in the analysis of gravity dam with a triangular load*

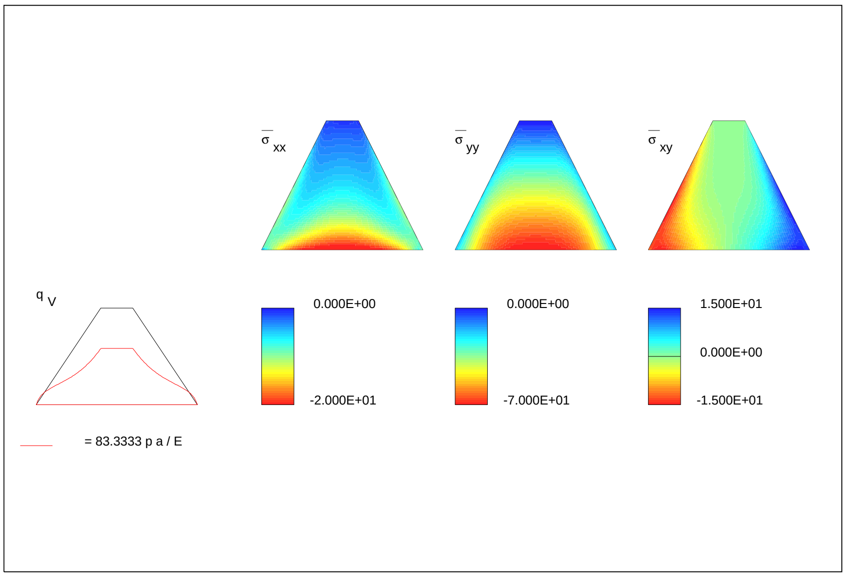

Figure 19: *Gravity dam with the self-weight applied*

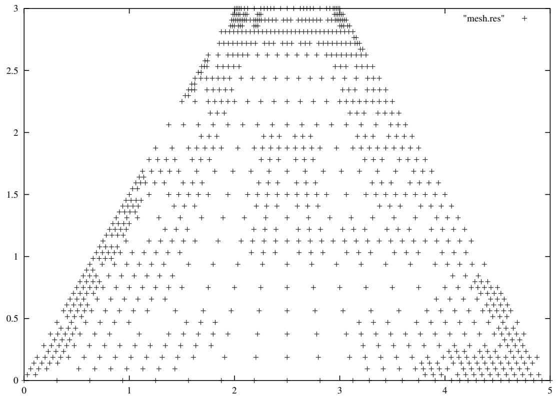

Figure 20: *Final non-uniform mesh in the analysis of gravity dam with self-weight load*

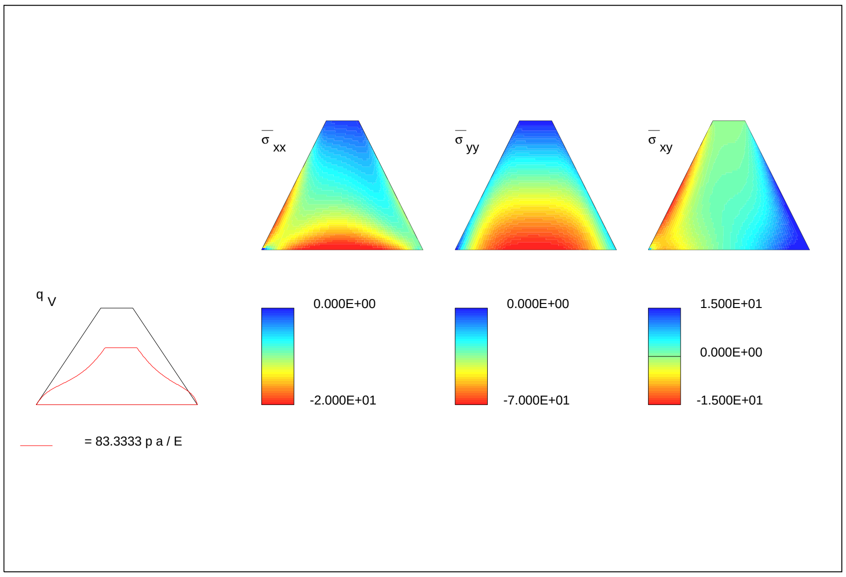

Figure 21: *Gravity dam with a triangular load and the self-weight applied*

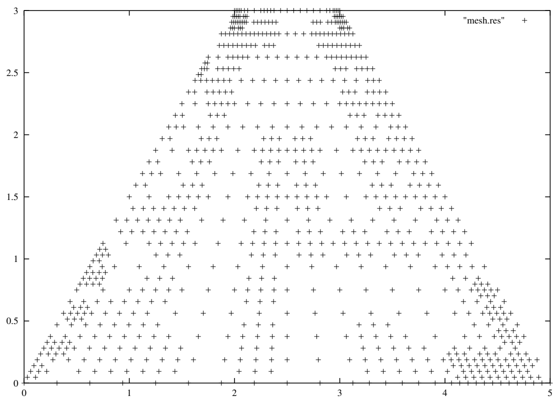

Figure 22: *Final non-uniform mesh in the analysis of gravity dam with a triangular and self-weight load*

degrees of freedom associated the final non-uniform grid. It indicates also the CPU times involved in computations.

Load case	N	j_0	j_{max}	n_{grid}	n_{dof}	T_{CPU}
1	4	3	6	536	1072	12.5
2	4	3	6	935	1870	48.5
3	4	3	6	846	1692	49.2

Table 6: Analysis of the gravity dam; final non-uniform grids

5 Conclusions and further developments

The examples presented in the previous section show clearly that the use of adaptive collocation techniques based on the use of interpolating wavelets is an attractive tool for the numerical analysis of plane elasticity problems.

In order to be able to deal with more realistic structural engineering problems, several aspects of the implementation must however be improved. For this purpose it is necessary:

- To implement a scheme that allows for the sub-division of the structure in sub-domains in order make possible the analysis of more complex geometries;

- To develop a suitable preconditioner for the iterative solution of the governing system that may be able to exploit the characteristics of the basis being used;
- To implement efficient IWT algorithms for the post-processing operations.

To exploit the advantages of the numerical schemes being discussed, it will be convenient to generalize the application of these techniques to other types of structural problems. It is being carried out now the implementation of a similar adaptive collocation scheme for the solution of Reissner-Mindlin plate bending problems, which is also a second order problem. It is also planned the development of a collocation technique for the solution of thin Kirchhoff plate bending problems (a fourth order problem).

Finally, it will be necessary to include in the algorithm the possibility of taking into account the physical non-linearities presented in the representation of the material behavior. It is then necessary to use the Plasticity Theory for ductile materials (such as metals) or the Continuum Damage Theory for quasi-brittle materials (such as concrete).

Acknowledgements

This work has been supported by the EC through research programme TMR-ERBFMRXCT-98-0184, “Wavelets in Numerical Analysis and Simulation”. It was partially supported also by ICIST (of which Luis Castro is member) and by PRAXIS XXI as part of research project 2/2.1/CEG/33/94.

References

[1] Bank, R.E., and Smith, R.K., Some a posteriori error estimates for elliptic partial differential equations. *Comput. Meth. Appl. Mech. Engrg.* **61**:283–301, 1987.

[2] Bertoluzza, S., Adaptive wavelet collocation method for the solution of Burgers equation, *Trans. Th. Stat. Phys.* **25**, 1996.

[3] J. R. Barber, *Elasticity*, Solid Mechanics and Its Applications, Kluwer Academic Publishers, Dordrecht, (1992);

[4] S. Bertoluzza, *An Adaptive Collocation Method based on Interpolating Wavelets*, in "Multiscale Wavelet Methods for Partial Differential Equations", edited by Dahmen, Kurdila and Oswald, Academic Press, 1997;

[5] S. Bertoluzza, J.C. Ravel, and Y. Maday. A dynamically adaptive wavelet method for solving pertial differential equations. *Comput. Methods Appl. Mech. Engrg.*, 1994.

[6] S. Bertoluzza and P. Pietra, Adaptive Wavelet Collocation for nonlinear BVPs, *Lecture Notes in Control and Information Sciences*, Springer Verlag, London (1996).

[7] G. Beylkin and N. Saito, Multiresolution representations using the auto-correlation functions of compactly supported wavelets, *IEEE Trans. Signal Processing*, **41**:3584-3590, 1993.

[8] A. Cohen, W. Dahmen, and R. De Vore. Adaptive wavelet methods for elliptic operator equations – convergence rates. Technical report, IGPM - RWTH-Aachen, 1998. to appear in Math. Comp.

[CDV93] A. Cohen, I. Daubechies, and P. Vial. Wavelets on the interval and fast wavelet transforms. *ACHA*, 1:54–81, 1993.

[9] COSMOS/M, *Finite Element System*, Version 1.70, Structural Research and Analysis Corporation, (1993);

[10] I. Daubechies, *Orthonormal Bases of Compactly Supported Wavelets*, Communications on Pure and Applied Mathematics, vol. 41, pp. 909-996, (1988);

[11] Interpolation Dyadique. In Fractals, dimensions non entieres et applications. Masson, Paris, 1987, pp. 44–55.

[12] Donoho, D., Interpolating Wavelet Transform, Department of Statistics, Stanford University, 1992, preprint.

[13] Dahmen, W. Stability of Multiscale Transformation, *Jour. of Fourier Anal. and Appl.*

[14] Erikson, K., and Johnson C., Adaptive Streamline Diffusion Finite Element Method for stationary Convection-Diffusion Problems, *Math. of Comp.* **60**:167–188, 1991.

[15] J.A. Teixeira de Freitas, J.P. Moitinho de Almeida and E.M.B. Ribeiro Pereira, Non-conventional formulations for the finite element method, *Structural Engineering and Mechanics*, 4, pp. 655-678, 1996.

[16] J.A. Teixeira de Freitas, J.P. Moitinho de Almeida and E.M.B. Ribeiro Pereira, Non-conventional formulations for the finite element method, *in* Modelling and Simulation Based Engineering, pp. 254-259, edited by S.N. Atlury and P.E. O'Donoghue, Palmdale, 1998.

[17] J. A. T. Freitas, *Duality and Symmetry in Mixed Integral Methods of Elastostatics*, International Journal for Numerical Methods in Engineering, Vol. 28, pp. 1161-1179, (1989);

[18] J. A. T. Freitas e E. M. B. R. Pereira, *O Método dos Integrais de Fronteira Usando Séries de Fourier*, MECOM89, X Congresso Ibero-Latino-Americano sobre Métodos Computacionais em Engenharia, Vol. 1, A221-A230, Porto, (1989);

[19] J. P. B. Moitinho de Almeida, *Janela: Uma interface gráfica destinada à aplicação em problemas de Mecânica Computacional*, Internal Report, Instituto Superior Técnico, Technical University of Lisbon, (1992);

[20] Y. Maday, V. Perrier, and J.C. Ravel. Adaptivité dynamique sur bases d'ondelettes pour l'approximation d'équations aux derivées partielles. *C. R. Acad. Sci Paris*, 312, (Série I):405–410, 1991.

[21] E. M. B. R. Pereira and J. A. T. Freitas, *A Mixed-Hybrid Finite Element Model Based on Orthogonal Functions*, International Journal for Numerical Methods in Engineering, Vol. 39, pp. 1295-1312, (1996);

[22] Rannacher, R., The dual-weighted-residual method for error control and mesh adaptation in finite element methods. *The mathematics of finite elements and applications, X, MAFELAP 1999 (Uxbridge)*, 97–116, Elsevier, Oxford, 2000.

[23] Koster, F., Griebel, M., Kevlahan, N. K.-R., Farge, M., and Schneider, K. Towards an adaptive wavelet-based 3D Navier-Stokes solver. *Numerical flow simulation, I (Marseille, 1997), 339–364, Notes Numer. Fluid Mech.*, 66, Vieweg, Braunschweig, 1998.

[24] S. P. Timoshenko and J. N. Goodier, *Theory of Elasticity*, 3^{rd} edition, McGraw-Hill International Book Company, Tokyo, (1982);

[25] Vasilyev, O.V. and Bowman, C., Second Generation Wavelet Collocation Method for the Solution of Partial Differential Equations. *J. Comp. Phys.*, **165**:660-693, 2000.

[26] Vasilyev, O.V., and Paolucci, S., A Dynamically Adaptive Multilevel Wavelet Collocation Method for Solving Partial Differential Equations in a Finite Domain. *J. Comp. Phys.*, **125**:498-512, 1996.

[27] Verfürt, R., A Posteriori Error Estimation and adaptive Mesh Refinement Techniques, *J. Comput. Appl. Math.* **50**:67–83, 1994.

[28] J.L. Walsh, A closed set of orthogonal functions, *Ann J Math*, 55, pp. 5-24, 1923.

[29] O. C. Zienkiewicz e R. L. Taylor, *The Finite Element Method, Volume 1 - Basic Formulation and Linear Problems*, 4^{rd} edition, McGraw-Hill Book Company, Berkshire, (1989);